Title
Optical and ultraviolet spectroscopic analysis of SN 2011fe at late times

Authors
Friesen, B
Baron, E
Parrent, JT
et al.

Peer Reviewed

Title:
Optical and ultraviolet spectroscopic analysis of SN 2011fe at late times

Journal Issue:
Monthly Notices of the Royal Astronomical Society, 467(2)

Author:
Friesen, B
Baron, E
Parrent, JT
Thomas, RC
Branch, D
Nugent, PE
Hauschildt, PH
Foley, RJ
Wright, DE
Pan, YC
Filippenko, AV
Clubb, KI
Silverman, JM
Maeda, K
Shivvers, I
Kelly, PL
Cohen, DP
Rest, A
Kasen, D

Publication Date:
01-01-2017

Series:
UC Santa Cruz Previously Published Works

Also Available:
Recent Work

Permalink:
http://escholarship.org/uc/item/8qb15891

Abstract:

© 2017 The Authors. We present optical spectra of the nearby Type Ia supernova SN 2011fe at 100, 205, 311, 349 and 578 d post-maximum light, as well as an ultraviolet (UV) spectrum obtained with the Hubble Space Telescope at 360 d post-maximum light. We compare these observations with synthetic spectra produced with the radiative transfer code PHOENIX. The day +100 spectrum can be well fitted with models that neglect collisional and radiative data for forbidden lines. Curiously, including these data and recomputing the fit yields a quite similar spectrum, but with different combinations of lines forming some of the stronger features. At day +205 and later epochs, forbidden lines dominate much of the optical spectrum formation; however, our results indicate that recombination, not collisional excitation, is the most influential physical process driving spectrum formation at these late times. Consequently, our synthetic optical and UV spectra at all epochs presented here are formed almost exclusively through recombinationdriven fluorescence. Furthermore, our models suggest that the UV spectrum even as late as day +360 is optically thick and consists of permitted lines from several iron-peak species. These results indicate that the transition to the 'nebular' phase in Type Ia supernovae is complex and highly wavelength dependent.

Copyright Information:

Optical and ultraviolet spectroscopic analysis of SN 2011fe at late times

Brian Friesen,[1,2] E. Baron,[1,3,4]★ Jerod T. Parrent,[5] R. C. Thomas,[2] David Branch,[1] Peter E. Nugent,[3] Peter H. Hauschildt,[4] Ryan J. Foley,[6,7,8] Darryl E. Wright,[9] Yen-Chen Pan,[7,8] Alexei V. Filippenko,[10] Kelsey I. Clubb,[10] Jeffrey M. Silverman,[11]† Keiichi Maeda,[12,13] Isaac Shivvers,[10] Patrick L. Kelly,[10] Daniel P. Cohen,[10] Armin Rest[14,15] and Daniel Kasen[10,16,17]

[1]*Homer L. Dodge Department of Physics & Astronomy, 440 W. Brooks St, Rm 100, Norman, OK 73019, USA*
[2]*NERSC, Lawrence Berkeley National Laboratory, 1 Cyclotron Road, MS 59R4010A, Berkeley, CA 94720, USA*
[3]*Computational Research Division, Lawrence Berkeley National Laboratory, 1 Cyclotron Road MS 50B-4206, Berkeley, CA 94720, USA*
[4]*Hamburger Sternwarte, Gojenbergsweg 112, D-21029 Hamburg, Germany*
[5]*Harvard-Smithsonian Center for Astrophysics, 60 Garden Street, Cambridge, MA 02138, USA*
[6]*Department of Astronomy and Astrophysics, University of California, Santa Cruz, CA 95064, USA*
[7]*Astronomy Department, University of Illinois at Urbana-Champaign, 1002 West Green Street, Urbana, IL 61801, USA*
[8]*Department of Physics, University of Illinois Urbana-Champaign, 1110 West Green Street, Urbana, IL 61801, USA*
[9]*Astrophysics Research Centre, School of Mathematics and Physics, Queen's University Belfast, Belfast BT7 1NN, UK*
[10]*Department of Astronomy, University of California, 501 Campbell Hall, Berkeley, CA 94720, USA*
[11]*Department of Astronomy, University of Texas at Austin, Austin, TX 78712, USA*
[12]*Department of Astronomy, Kyoto University, Kitashirakawa-Oiwake-cho, Sakyo-ku, Kyoto 606-8502, Japan*
[13]*Kavli Institute for the Physics and Mathematics of the Universe, University of Tokyo, 5-1-5 Kashiwanoha, Kashiwa, Chiba 277-8583, Japan*
[14]*Department of Physics, Harvard University, 17 Oxford Street, Cambridge, MA 02138, USA*
[15]*Space Telescope Science Institute, 3700 San Martin Drive, Baltimore, MD 21218, USA*
[16]*Department of Physics, University of California, 366 LeConte Hall MC 7300, Berkeley, CA 94720, USA*
[17]*Nuclear Science Division, Lawrence Berkeley National Laboratory, 1 Cyclotron Road, Berkeley, CA 94720, USA*

ABSTRACT

We present optical spectra of the nearby Type Ia supernova SN 2011fe at 100, 205, 311, 349 and 578 d post-maximum light, as well as an ultraviolet (UV) spectrum obtained with the *Hubble Space Telescope* at 360 d post-maximum light. We compare these observations with synthetic spectra produced with the radiative transfer code PHOENIX. The day +100 spectrum can be well fitted with models that neglect collisional and radiative data for forbidden lines. Curiously, including these data and recomputing the fit yields a quite similar spectrum, but with different combinations of lines forming some of the stronger features. At day +205 and later epochs, forbidden lines dominate much of the optical spectrum formation; however, our results indicate that recombination, not collisional excitation, is the most influential physical process driving spectrum formation at these late times. Consequently, our synthetic optical and UV spectra at all epochs presented here are formed almost exclusively through recombination-driven fluorescence. Furthermore, our models suggest that the UV spectrum even as late as day +360 is optically thick and consists of permitted lines from several iron-peak species. These results indicate that the transition to the 'nebular' phase in Type Ia supernovae is complex and highly wavelength dependent.

Key words: supernovae: general – supernovae: individual: SN 2011fe.

1 INTRODUCTION

The Type Ia supernova (SN Ia) SN 2011fe was discovered on 2011 August 24 (UT dates are used throughout this paper), just 11 h after explosion (Nugent et al. 2011; but also see Piro & Nakar 2014 and Mazzali et al. 2011). It is among the nearest (∼6.9 Mpc) and

---

★ E-mail: baron@ou.edu
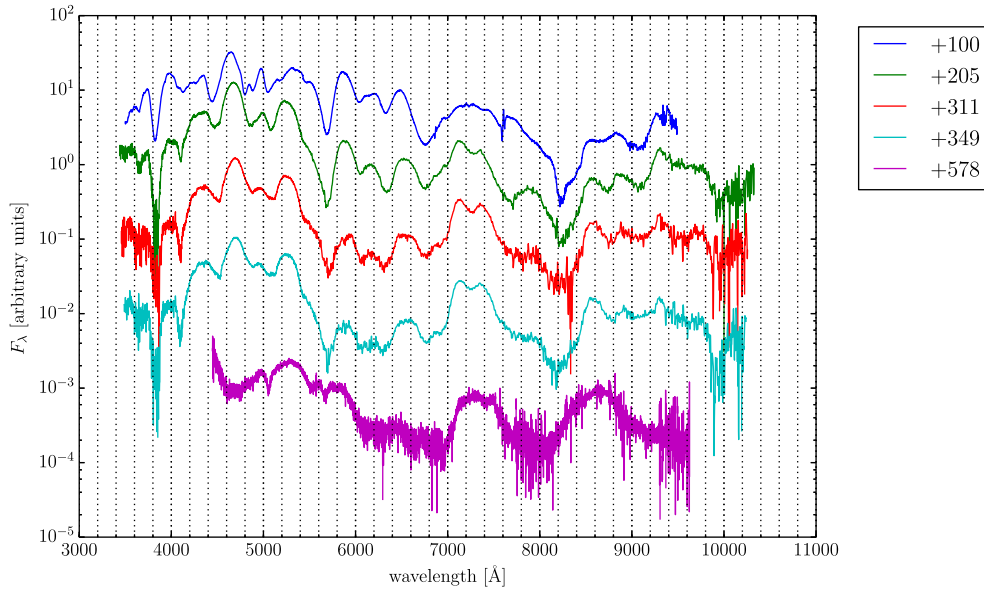† NSF Astronomy, Astrophysics Postdoctoral Fellow.

Figure 1. Five optical spectra of SN 2011fe used in this work. The fluxes are scaled arbitrarily in order to facilitate spectral feature comparisons. In this and all subsequent plots, the wavelengths are plotted in the observed frame.

youngest (∼11 h) Type Ia supernovae (SNe Ia) ever discovered. Extensive spectroscopic and photometric studies of SN 2011fe indicate that it is 'normal' in nearly every sense: in luminosity, spectral and colour evolution, abundance patterns, etc. (Parrent et al. 2012; Richmond & Smith 2012; Röpke et al. 2012; Vinkó et al. 2012; Munari et al. 2013; Pereira et al. 2013; Mazzali et al. 2014). Its unremarkable nature coupled with the wealth of observations made over its lifetime render it an ideal laboratory for understanding the physical processes that govern the evolution of normal SNe Ia. Indeed, these data have allowed observers to place numerous and unprecedented constraints on the progenitor system of a particular SN Ia (e.g. Li et al. 2011; Nugent et al. 2011; Bloom et al. 2012; Chomiuk et al. 2012; Horesh et al. 2012; Margutti et al. 2012).

Equally as information-rich as observations taken at early times are those taken much later, when the SN's photosphere has receded and spectrum formation occurs deep in the SN core. For example, Shappee et al. (2013) used late-time spectra to further study the progenitor system of SN 2011fe, deducing an upper limit to the amount of hydrogen stripped from the putative companion of <0.001 M$_\odot$. Further analysis by this group found no trace of [O I] λ6300 or [Ca II] λλ7291, 7324 emission lines, leading to even smaller upper limits (Lundqvist et al. 2015). McClelland et al. (2013) found that the luminosity from SN 2011fe in the 3.6-μm channel of *Spitzer*/IRAC fades almost twice as quickly as in the 4.5-μm channel, which they argue is a consequence of recombination from doubly ionized to singly ionized iron-peak elements. In addition, Kerzendorf et al. (2014) used photometric observations near 930 d post-maximum light to construct a late-time quasi-bolometric light curve and showed that the luminosity continues to trace the radioactive decay rate of ^{56}Co quite closely, suggesting that positrons are fully trapped in the ejecta, disfavouring a radially combed or absent magnetic field in this SN. Graham et al. (2015) presented an optical spectrum at 981 d post-explosion and used constraints on both the mass of hydrogen and the luminosity of the putative secondary star as evidence against a single-degenerate explosion mechanism. Taubenberger et al. (2015) presented an optical spectrum at 1034 d post-explosion and speculated about the presence of [O I] lines near 6300 Å, which, if confirmed, would provide strong constraints on the mass of unburned

Table 1. Observing log of spectra that appear here for the first time. The phase is with respect to maximum light.

UT Date	Phase (d)	Telescope +Instrument
2011 December 19	+100	WHT+ISIS
2012 April 2	+205	Lick 3-m+Kast
2012 July 17	+311	Lick 3-m+Kast
2012 August 23	+349	Lick 3-m+Kast
2013 April 8	+578	Lick 3-m+Kast

material near the centre of the white dwarf progenitor of SN 2011fe. Non-detections of the Hα line at both of these very late epochs also strengthened the constraints on the presence of hydrogen initially posed by Shappee et al. (2013). Graur, Maoz & Shara (2014) used *Hubble Space Telescope* (*HST*) observations to look at the region ∼1 yr prior to explosion and found no evidence of He II emission that should be produced by the hard radiation from an accreting white dwarf. Finally, Mazzali et al. (2015) used spectrum synthesis models of SN 2011fe from 192 to 364 d after explosion to argue for a large central mass of stable iron and a small mass of stable nickel – about 0.23 M$_\odot$ and 0.01 M$_\odot$, respectively.

We complement these various late-time analyses with radiative transfer models corresponding to a series of optical and ultraviolet (UV) spectra of SN 2011fe.

2 OBSERVATIONS

We obtained optical spectra of SN 2011fe at days +100, +205, +311, +349 and +594 (2011 December 19; 2012 April 2; 2012 July 17; 2012 August 23; 2013 March 27); the data are shown in Fig. 1 and described in Table 1. The day +205 and +311 spectra were presented by Mazzali et al. (2015). We also obtained a UV spectrum with *HST* at day +360 (GO-12948; PI: R. Thomas). This latter observation consisted of 10 orbits, the first 9 using the STIS/NUV-MAMA configuration and the last with the STIS/CCD G430L and G750L configurations. The data from one of the NUV-MAMA
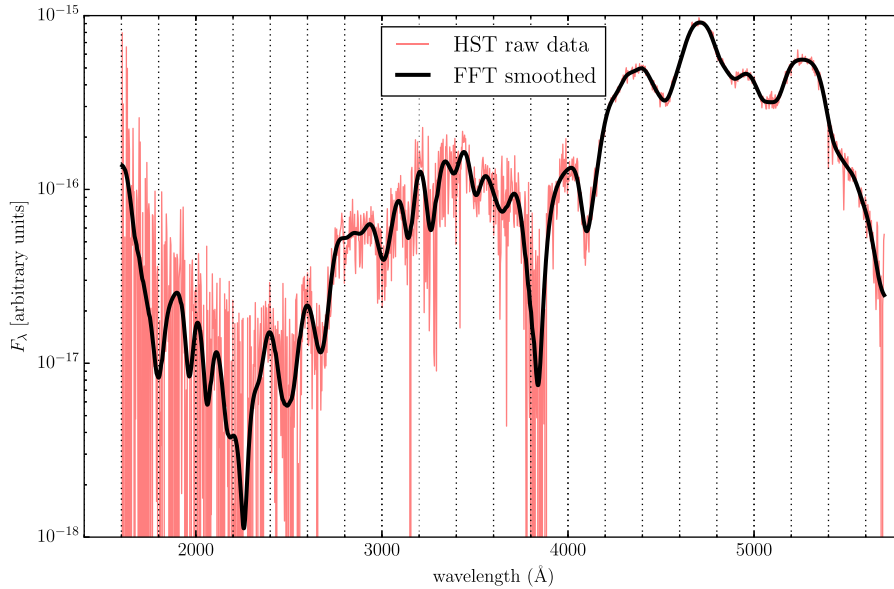
Figure 2. *HST* CCD+MAMA spectrum of SN 2011fe at day +360. The smoothed spectrum uses the low-pass filter technique outlined by Marion et al. (2009).

orbits were unrecoverable, so the final spectrum, shown in Fig. 2, represents coaddition of the nine remaining observations.

Also shown in Fig. 2 is a smoothed version of the *HST* spectrum. We used the algorithm presented by Marion et al. (2009), which consists of applying a low-pass filter to the signal. The motivation for this approach is the notion that the physical features in SN Ia spectra are broad, while most noise in the spectrum is narrow. Therefore, if one can suppress the high-'frequency' features (the noise), what remains is the pure signal from the SN. To accomplish this task, one calculates the power spectrum of the original spectrum using a Fourier transformation, suppresses the power spectrum at all high 'frequencies' in which information is deemed to be noise, and applies an inverse Fourier transformation to recover the smoothed spectrum. An especially useful feature of this technique is its insensitivity to spikes in *HST* spectra produced by cosmic rays.

3 RADIATIVE TRANSFER MODELS

We used the PHOENIX/1D code (Hauschildt & Baron 1999) with the same modifications discussed by Friesen et al. (2014) to capture the most important physical processes at late times in SNe Ia. The underlying explosion model was a spherically symmetric delayed-detonation model presented by Domínguez, Höflich & Straniero (2001). For each observation presented in Section 2, we calculated a corresponding synthetic spectrum, assuming a 16 d rise time for the model (Nugent et al. 2011). The abundance structure of the explosion model is shown in Fig. 3. The results are in broad agreement with those of Mazzali et al. (2015), who find a nickel hole and stratified composition.

4 DISCUSSION

The theory of spectrum formation at late times in normal SNe Ia has broadly converged to a scenario in which electron configurations of atoms in the rarefied ejecta are primarily in their ground state, and are excited by collisions with free electrons to low-lying metastable levels, which in turn emit forbidden lines as they return to the ground state (e.g. Meyerott 1978, 1980; Axelrod 1980; Ruiz-Lapuente &
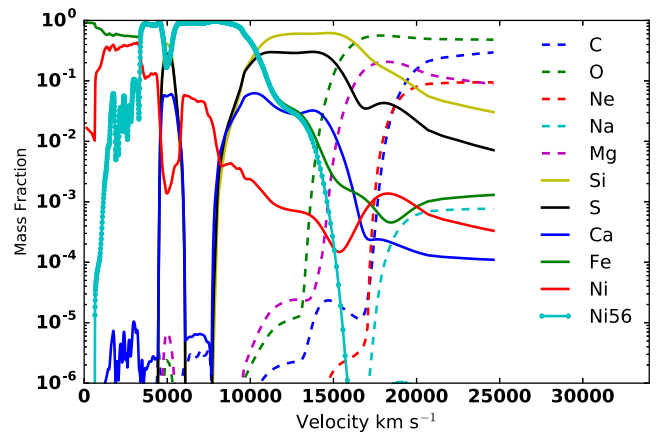

Figure 3. The abundances at time $t = \infty$ for the delayed-detonation model of Domínguez et al. (2001). The ^{56}Ni abundance is given at time $t = 0$.

Lucy 1992; Kuchner et al. 1994; Ruiz-Lapuente et al. 1995; Bowers et al. 1997; Mazzali et al. 2011; Mazzali & Hachinger 2012; Silverman, Ganeshalingam & Filippenko 2013). Little to no continuum emission is present in SN Ia spectra at these epochs. This stands in contrast to the spectrum formation mechanism at early times, near maximum light, in which the optical depth to Thomson scattering on free electrons is large, leading to the formation of a photosphere on top of which atoms undergo line scattering via strong permitted lines, giving rise to P Cygni spectral features. The physics of nebular spectrum formation was first laid out by Meyerott (1978), Meyerott (1980) and Axelrod (1980).

Kirshner & Oke (1975) argued that the P Cygni mechanism is no longer active at late times because the photosphere has disappeared (indicated by the absence of a continuum) and there are no longer enough photons for these strong lines to scatter.

Curiously, good spectral fits have been obtained for post-photospheric SN Ia spectra with the parametrized spectrum synthesis code SYNOW, which treats only line scattering by permitted lines. Such fits require only a few ions – Na I, Ca II and Fe II – and fit
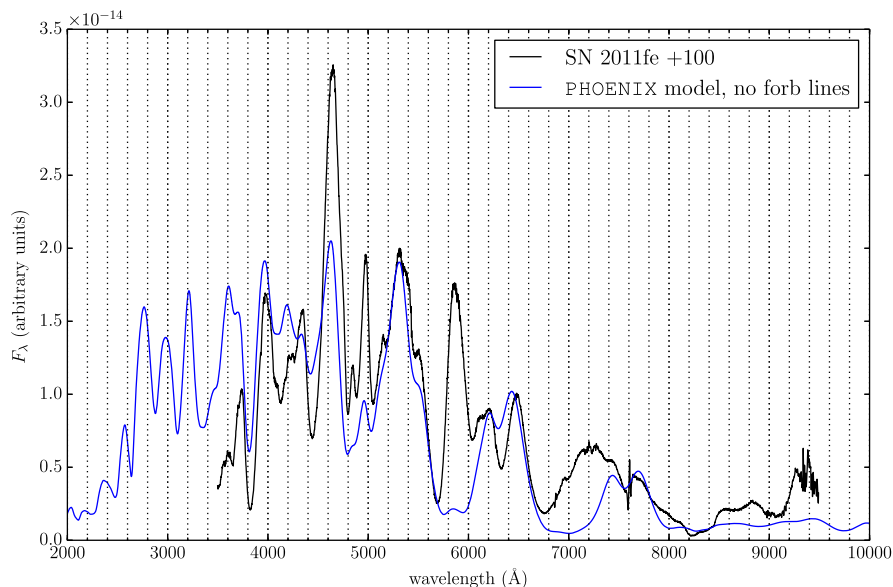
Figure 4. Synthetic spectrum of delayed-detonation model of Domínguez et al. (2001) at day 116 versus SN 2011fe at day +100. No forbidden lines were included in this calculation.
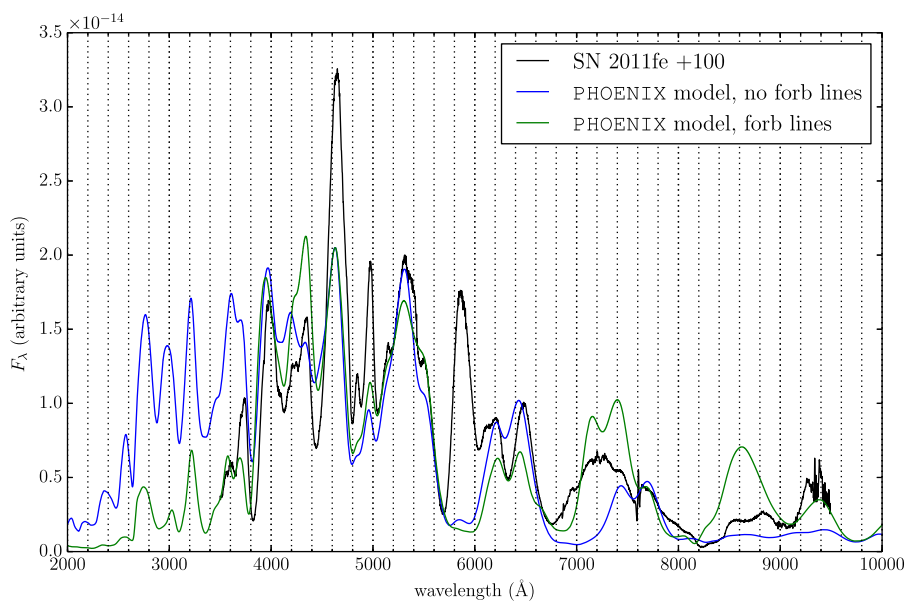

Figure 5. Comparison of PHOENIX spectra with and without forbidden lines at day +116.

optical spectra fairly well, especially blueward of ∼6000 Å. Examples include the normal SN 1994D at day +115 (Branch et al. 2005), the normal SN 2003du at day +84 (Branch et al. 2008), the subluminous SN 1991bg at day +91 (Branch et al. 2008) and the peculiar SN 2002cx at day +227 (Jha et al. 2006). While the parametrized approach of SYNOW to solving the radiative transfer equation restricts analysis of those fits to putative line identifications and velocity measurements, they nevertheless demonstrate that either SN Ia spectra exhibit a remarkable degeneracy with respect to forbidden and permitted line formation, or that permitted lines continue to drive emergent spectrum formation at post-photospheric epochs, regardless of what physical mechanisms generate the underlying flux (Branch et al. 2008; Friesen et al. 2012).

These two competing analyses of late-time SN Ia spectra agree that the majority of the spectrum is formed by Fe lines, but they

predict dramatically different velocities of the line-forming regions in the ejecta. For example, Branch et al. (2008) argue that Fe, Ca and Na are located at 7000 km s^{-1} and higher in the day +84 spectrum of SN 2003du. In contrast, Bowers et al. (1997) argue for velocities from 1000 to 3000 km s^{-1} in the +95 d spectrum of the same object. Identifying the correct velocity of the line-forming region has important consequences for constraining the structure of the inner regions of SN Ia ejecta, which in turn constrain the as-yet unknown explosion mechanism.

4.1 Day +100

The day +100 spectrum of SN 2011fe and the corresponding synthetic spectrum from PHOENIX are shown in Fig. 4. Overall, the fit is acceptable. The main discrepancy between our model and features
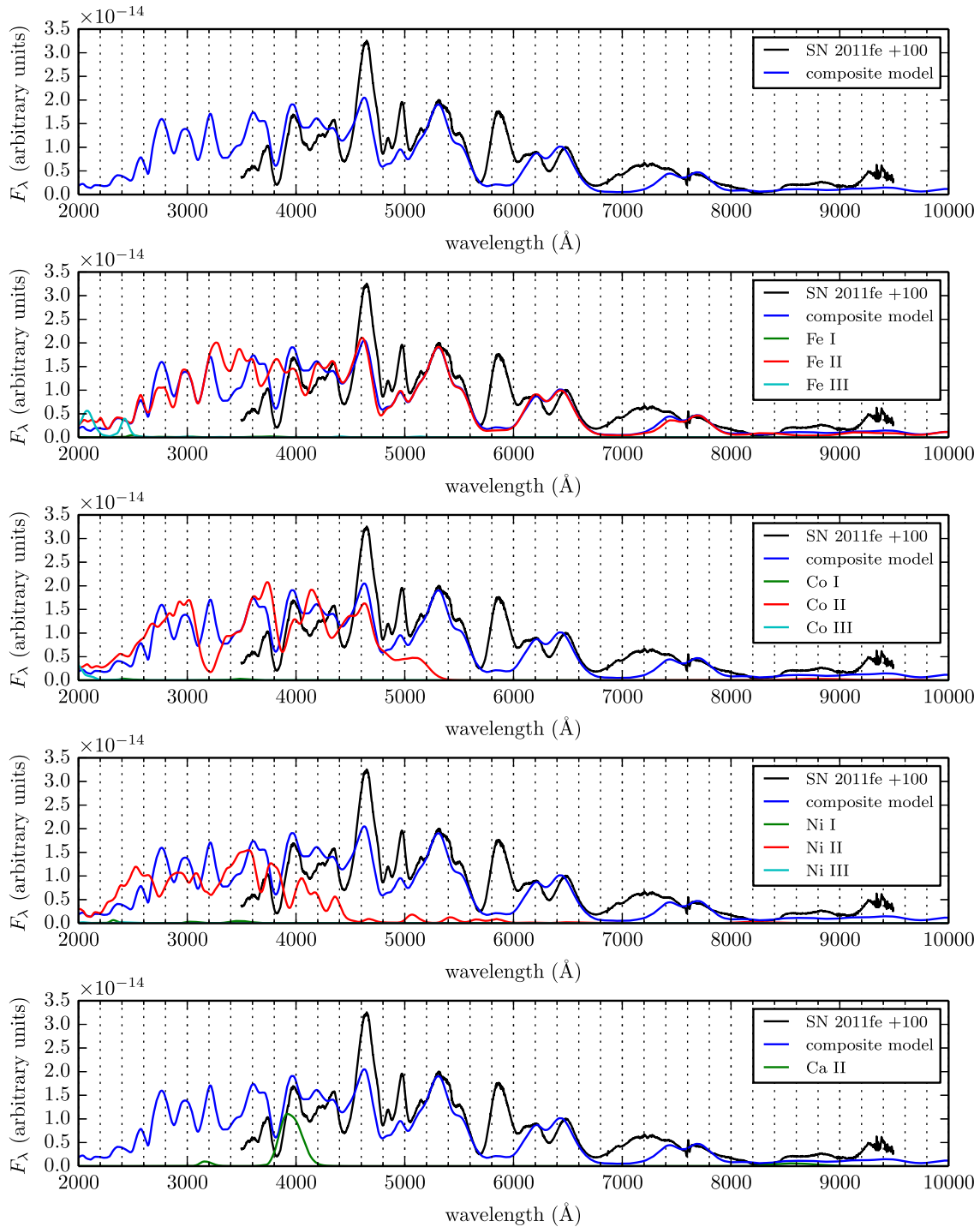
Figure 6. Single-ion spectra corresponding to the composite spectrum of the delayed-detonation model of Domínguez et al. (2001) at day +116 compared to SN 2011fe at day +100. No forbidden lines were included in this calculation.

in the observed spectrum is the emission feature near 5900 Å. In addition, the peak at 4700 Å in the synthetic spectrum is too weak, the blue side of the broad emission at 7200 Å is absent in the model, and the flux in the blue and near-UV is too high. Most other features are well reproduced, both in strength and in shape.

In the context of much of the literature that concerns late-time SN Ia spectra, the fidelity of this fit is peculiar because the calculation used the most current atomic data base of Kurucz (1995, 2002), which includes no forbidden-line data for any ions. This stands in

contrast to the most common interpretations of spectra of 'old' SNe Ia, which were discussed earlier. If the purely permitted-line identifications are correct, they are difficult to reconcile with kinematic analyses such as that of Maeda et al. (2010), which assume that the emission peaks correspond to forbidden lines forming within a few 100 km s^{-1} of $v \approx 0$ km s^{-1}. Rather, the strong emission peaks at 4700 and 5200 Å, which each have previously been identified as a mixture of [Fe II] and [Fe III] lines, may instead be formed by the handful of permitted lines of Fe II whose upper levels are among
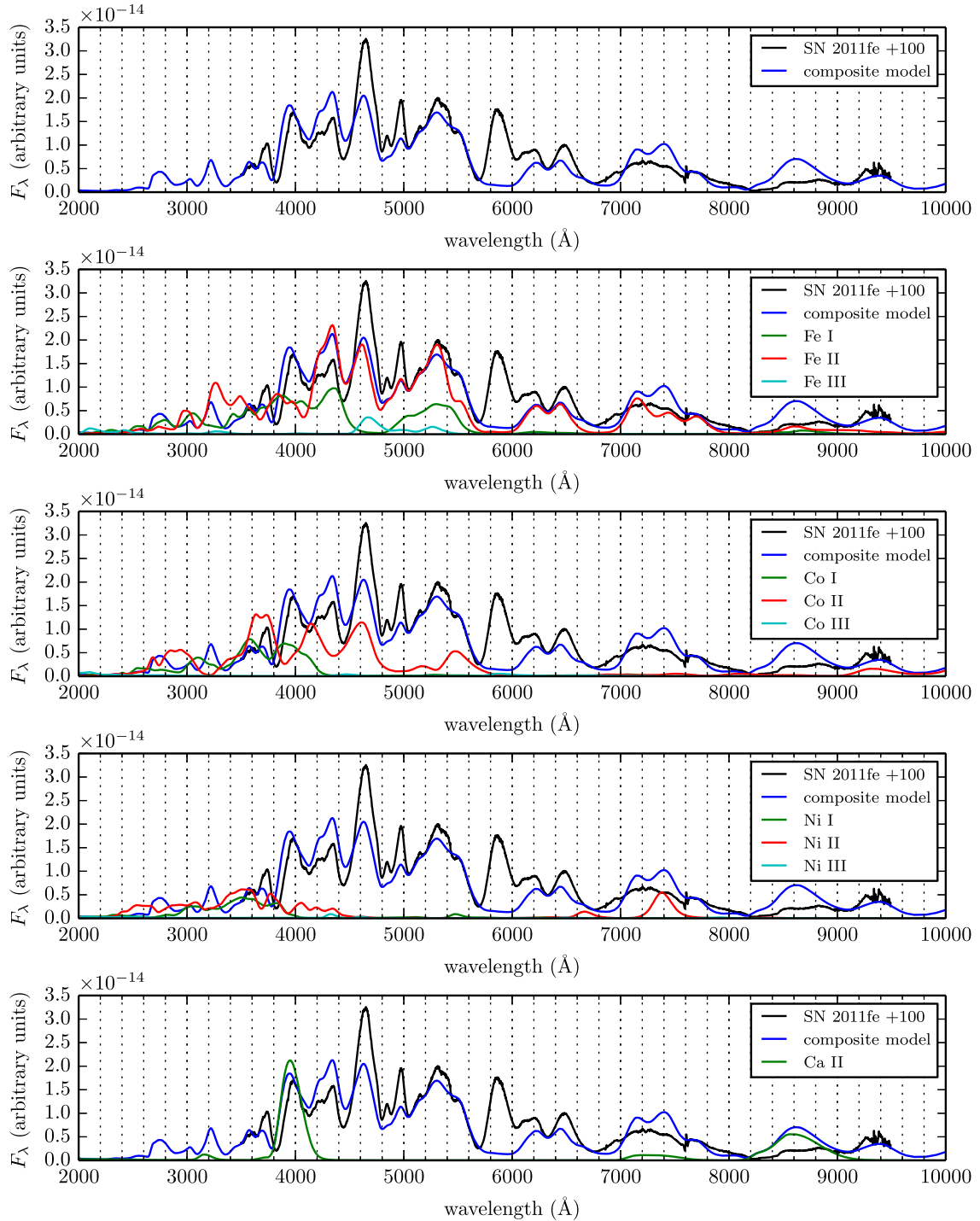
Figure 7. Single-ion spectra corresponding to the composite spectrum of the delayed-detonation model of Domínguez et al. (2001) at day +116 compared to SN 2011fe at day +100. Permitted and forbidden lines were included in this calculation.

the crowded $3d^6(^5D)4p$ configuration, with energies between 5 and 6 eV, and whose lower levels are, coincidentally, the handful of metastable levels around 3 eV that are purportedly responsible for the aforementioned forbidden emission features. The 5200 Å feature is identified as being due to a combination of [Fe II] lines at 5159, 5262, 5333 Å and [Fe III] at 5270 Å by Mazzali et al. (2015). Bowers et al. (1997) identified this feature as a blend of [Fe II] lines at 5159 Å and [Fe III] at 5270 Å.

It is important to note that the analysis of Maeda et al. (2010) only requires that the ejecta are optically thin at the rest wavelength of the line, and as we show below, in the redder parts of the spectra that condition is met at later epochs. Indeed, Maeda et al. (2011) showed observationally that the feature at ∼4700 Å, which is typically assumed to be a blend of [Fe III], should either suffer from radiation transfer effects or contamination from other lines for a long time, and thus they suggested that this feature should not be
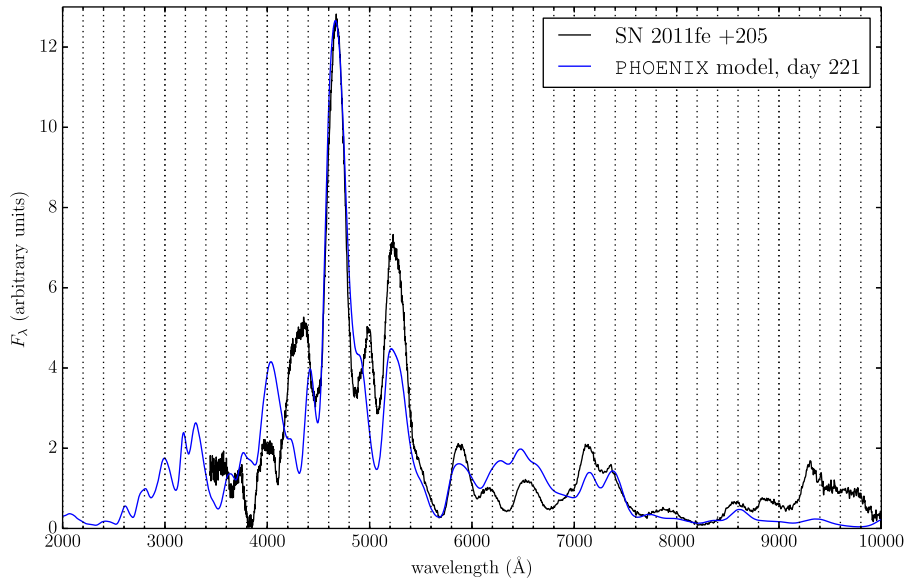
Figure 8. Synthetic spectrum of delayed-detonation model of Domínguez et al. (2001) at day +221 versus SN 2011fe at day +205. Permitted and forbidden lines were included in this calculation.

used for kinematic studies until about a year after the explosion. In the line-scattering interpretation of spectrum formation, this would imply that the dips just to the blue of these two strong emission features are the corresponding absorptions, rather than regions lacking in emission. These absorptions would correspond to line velocities of ∼6000 km s⁻¹, similar to that found in the +115 spectrum of SN 1994D by Branch et al. (2005). Optically thick permitted lines would produce true P Cygni profiles with blueshifted absorption and rest-wavelength emission, although even more complex shapes are possible (Friesen et al. 2012).

Although below we illustrate some complications with this permitted-line-only model, it is instructive first to entertain the idea that this is, in fact, representative of late-time spectrum formation physics in SNe Ia. Given the contrast of this result with those found elsewhere in the literature, it is important to evaluate the late-time line-scattering scenario within the context of other analyses of SN 2011fe, in order to determine whether it is consistent with what is already known about the spectral evolution of this object. We consider three such pieces of analysis. First, Parrent et al. (2012) traced the velocity evolution of Fe II in the early-time spectra of SN 2011fe using the automated spectrum code SYNAPPS (Thomas, Nugent & Meza 2011) and found that at day +15 the minimum velocity of that ion was ∼8000 km s⁻¹ (see fig. 3). Furthermore, after maximum light, the rate of change of line velocities in SN 2011fe, and in most SNe Ia in general, slows dramatically. Second, in the hydrodynamical model used in our calculation, Fe remains the most abundant species in the ejecta from the centre of the ejecta out to ∼12 000 km s⁻¹ (see Friesen et al. 2014, Fig. 2); our putative line-velocity estimate of ∼6000 km s⁻¹ falls well within this range. Finally, Iwamoto et al. (1999) show that the optical depth of Fe II computed in local thermodynamic equilibrium (LTE) peaks between 5000 and 10 000 K, roughly the same temperature range as that of the ejecta in our models. (One would remiss to read too much into this corroboration, as the radiation field in the SN Ia ejecta at this epoch is far from LTE.) Although none of these results offers conclusive evidence that the strong features in the +100 d spectrum of SN 2011fe are indeed P Cygni profiles, they do show that it is quite reasonable to consider that possibility.

We caution that it is unlikely that the *entire* optical spectrum consists of overlapping P Cygni line profiles due to resonance-scattering, as is the case at very early (photospheric) epochs in SNe Ia. Branch et al. (2008) attempted to fit the day +84 spectrum of SN 2003du with the resonance-scattering code SYNOW, and found that P Cygni lines fit the blue part of the spectrum (blueward of 6600 Å) quite well, but failed quite severely redward of that. As they discuss, the likely explanation is that resonance scattering near this epoch is very influential at blue wavelengths, but forbidden emission is prominent in the red. (We find a similar result in our attempts to fit the optical and UV spectra at +349 d and +360 d, respectively, which we discuss below.) In fact, to argue that spectrum formation consists of *either* resonance scattering by optically thick permitted lines *or* emission from optically thin forbidden lines is somewhat of a false dilemma, as both scenarios assume a degree of locality in the radiative transfer which is probably unphysical. In particular, the former assumes that the source function *S* depends only on the local mean intensity *J*, while the latter assumes that emitting lines are well separated in wavelength such that they act independently of each other. Each of these approximations is valid in certain regimes: resonance-scattering at photospheric epochs and forbidden emission at *very* late times (>1 yr) and in wavelength regions far from the forest of iron-peak lines, such as the infrared, but there exists a wide range between those extremes, in which all of these effects compete to form the emergent spectrum.

Bongard et al. (2008) addressed this topic in detail by calculating a grid of PHOENIX spectra using the hydrodynamical model W7 (Nomoto, Thielemann & Yokoi 1984) at 20 d post-explosion. They found that even at very low velocities and high optical depth (τ > 3), the 'spectrum'[1] at those velocities is already highly non-Planckian, owing to line and continuum interactions of the radiation field with iron-peak elements deep in the core of the SN. The ions found at higher velocities, near the photosphere, then further distort this underlying spectrum through additional absorption, emission and line scattering, leading to an emergent spectrum containing a
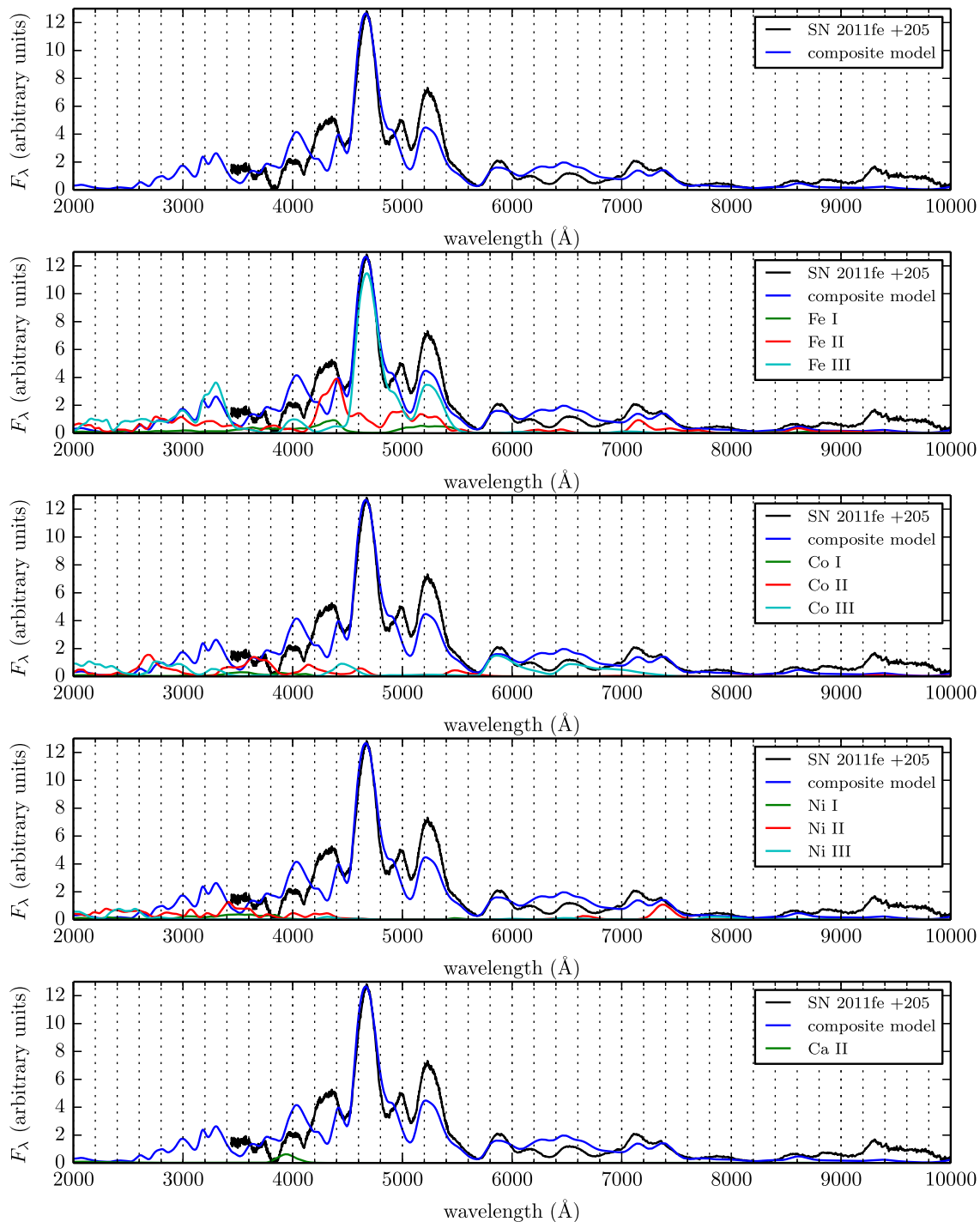
---

[1] The radiation flux F_λ.

Figure 9. Single-ion spectra corresponding to the composite spectrum of the delayed-detonation model of Domínguez et al. (2001) at day +221 compared to SN 2011fe at day +205. Permitted and forbidden lines were included in this calculation.

complicated mixture of P Cygni, continuum and thermal components that are difficult to disentangle.

Our spectral model that explicitly omits forbidden-line data fits the day +100 spectrum of SN 2011fe reasonably well suggests that day +100 is simply too early for collisionally excited forbidden emission to be the primary driver of spectrum formation. It appears that line-scattering processes continue to contribute significantly, even this late in the lifetime of this SN. In short, there are many

physically motivated reasons to suspect that permitted lines play an important role in SN Ia spectrum formation at this epoch.

However, since forbidden lines are frequently identified in spectra of SNe Ia of this age, we tested this theory by expanding our atomic data base to include collisional and radiative data of forbidden lines, as described by Friesen et al. (2014). We then repeated the radiative transfer calculation with this expanded data base, and we compare the two results in Fig. 5. They are quite similar, except that the model
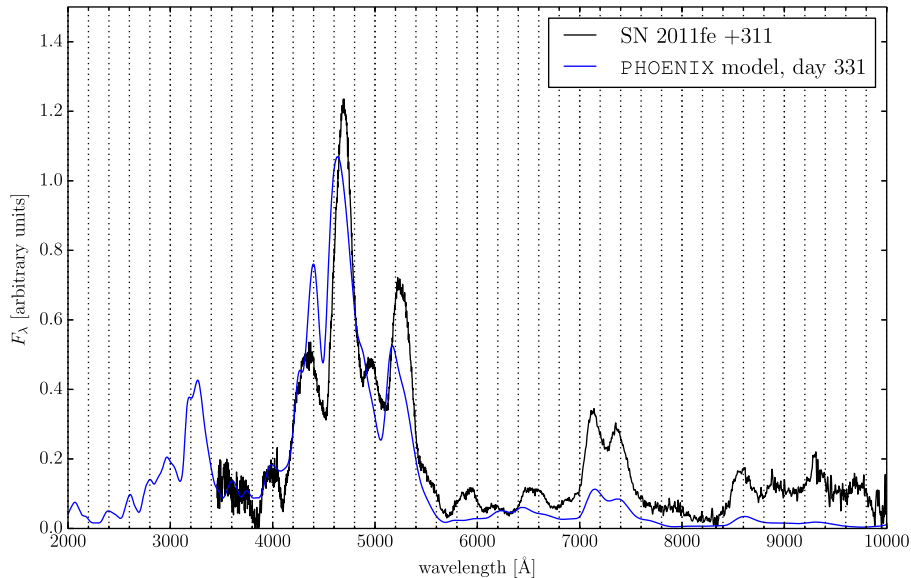
Figure 10. Synthetic spectrum of delayed-detonation model of Domínguez et al. (2001) at day +331 versus SN 2011fe at day +311. Permitted and forbidden lines were included in this calculation.

with forbidden lines has a lower UV flux and stronger emission at 7300 and 8600 Å.

The most notable shortcoming of both synthetic spectra is the lack of emission at 5900 Å. This feature has been identified alternatively as Na I D (Branch et al. 2008; Mazzali et al. 2008) or [Co III] $\lambda5888$ (Kuchner et al. 1994; Dessart et al. 2014; Childress et al. 2015). The explosion model used in these calculations contains little Na I, so it is not surprising that we do not recover a strong Na I D emission feature there. However, at day +116 the model contains several $0.1\,M_\odot$ of ^{56}Co, and yet the forbidden emission at 5900 Å does not appear. This discrepancy may be related to underestimating the gas temperature in the model at this epoch (see Section 4.2). At later times, the feature does appear clearly and is due to [Co III] $\lambda5888$; see below.

Identifying whether a feature is 'emission' or 'absorption' is not a straightforward task in PHOENIX calculations. This is because the algorithm calculates emissivities and opacities of non-LTE species by adding up all contributions to each at each wavelength point (e.g. Hauschildt & Baron 2014), with no regard to the underlying atomic processes that produced them. Such an approach captures naturally the notion that spectrum formation is inherently multilayered in SNe: one region deep in the ejecta may be strongly in emission at one wavelength, but a region above it may be optically thick at that wavelength, absorbing much of the underlying emission (Bongard et al. 2008). The emergent spectrum is then a convolution of both processes, and such classifications as 'absorption' or 'emission', while relevant to single interactions, no longer describe adequately the complete process of spectrum formation.

We are therefore relegated to using more indirect methods for isolating the sources of features in synthetic spectra. The single-ion spectrum method (Bongard et al. 2008) can help one identify the particular ion or ions that influence particular parts of a synthetic spectrum, but it cannot, for example, isolate the effects of permitted lines from forbidden lines, which is desirable in this context.

As described by Bongard et al. (2008), single-ion spectra are constructed as follows. Using the converged output of the PHOENIX simulation, we artificially turn off all line opacities except those for one single ion. The continuum opacities are unchanged and

include all of the bound-free and free–free opacities as well as electron and Rayleigh scattering. We then recalculate the solution of the scattering problem in order to get the 'single-ion spectrum', with the level populations, temperature structure and free-electron densities held fixed.

We found that the only useful way to accomplish this was to remove the forbidden lines from the calculation entirely and recompute the entire model. This can unfortunately broaden the parameter space of the model, since forbidden lines affect the temperature structure by acting as coolants (Dessart et al. 2014; Friesen et al. 2014). Unfortunately, we are aware of no more-targeted method of accomplishing this goal.

We computed single-ion spectra for both synthetic spectra (with and without forbidden lines), for the most influential ions. For the spectrum without forbidden lines, these are shown in Fig. 6. For the spectrum with forbidden lines, these are shown in Fig. 7.

Both with and without forbidden lines, the synthetic spectra indicate that most of the optical spectrum at day +100 is formed by Fe II. In addition, the Ca II H&K $\lambda\lambda3934$, 3968 doublet, a pair of strong resonance lines, contributes significantly to the emission at 4000 Å. However, comparison between the two sets of single-ion spectra indicates a fascinating result that Branch et al. (2008) found highly improbable: it appears that entirely different combinations of atomic lines can conspire to produce similar optical spectra. Furthermore, the synthetic spectra in Figs 4 and 5 are the *natural endpoints* of calculations subject to otherwise identical parameters. For example, when forbidden lines are included, the emission at 4000 Å is due entirely to the Ca II H&K doublet; when they are absent, it is a combination of that same doublet with contributions also from Fe II and Co II. The double-horned emissions at 7250 and 7500 Å in the synthetic spectra lacking forbidden lines are due to emission from Fe II, but the double-horned features at 7150 and 7400 Å in the spectra containing forbidden lines are due to Fe II (possibly [Fe II] $\lambda\lambda7155$, 7171) and [Ni II] $\lambda\lambda7374$, 7412.

This is likely stable ^{58}Ni, since the radioactive ^{56}Ni has mostly decayed by this point. The degeneracy among these various features is the probable explanation for the conflicting results of, for example, Bowers et al. (1997) and Branch et al. (2008).
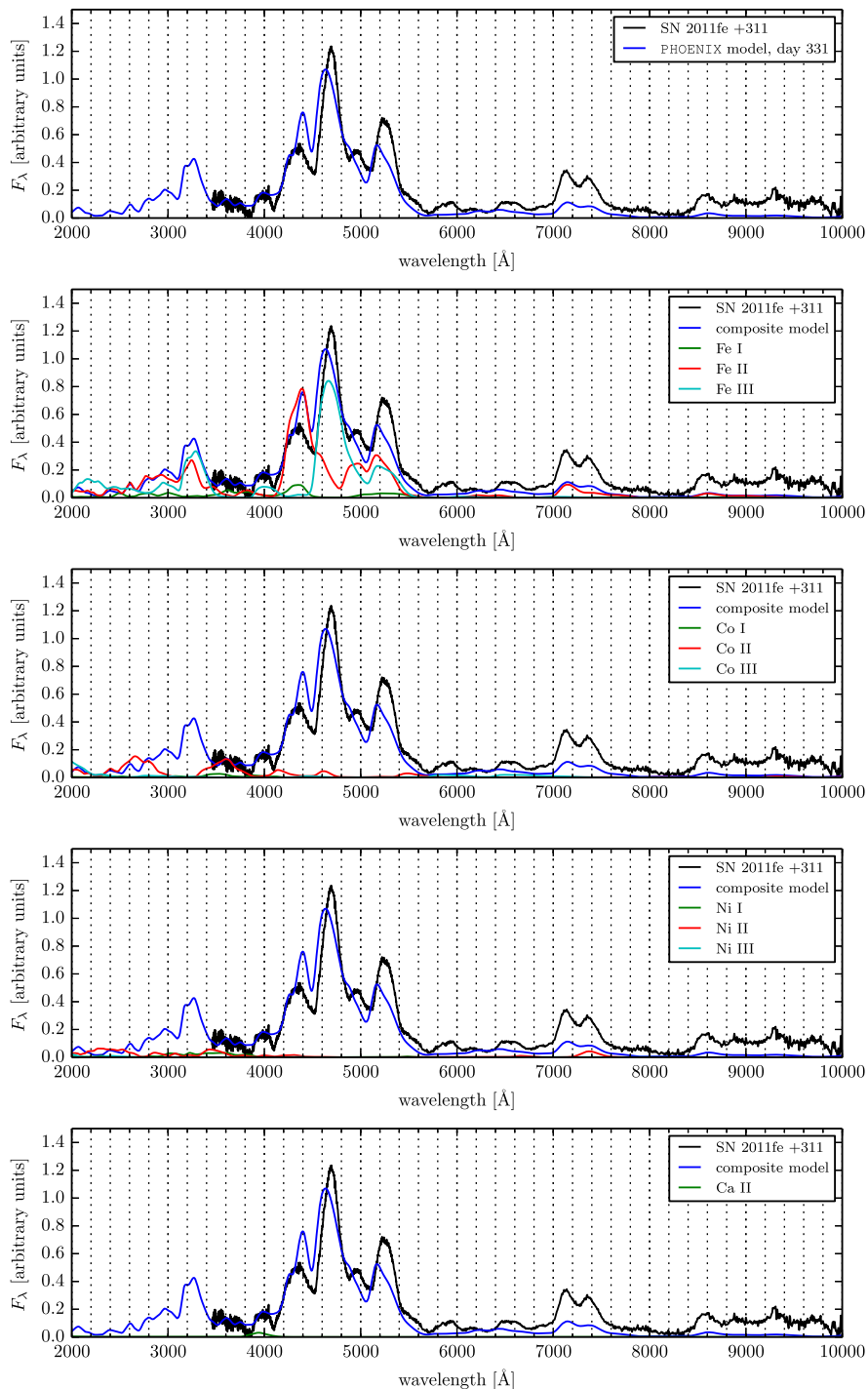
Figure 11. Single-ion spectra corresponding to the composite spectrum of the delayed-detonation model of Domínguez et al. (2001) at day +331 compared to SN 2011fe at day +311. Permitted and forbidden lines were included in this calculation.

One would expect that adding forbidden lines is always favourable over neglecting them: if a calculation captures all relevant atomic processes and if forbidden lines are truly unimportant in some scenario, they will naturally 'deactivate.' And in fact, adding in the forbidden atomic data did address some problems in the synthetic spectra that lacked them. The lower UV flux and the 8600 Å emission in the synthetic-spectrum forbidden lines can be explained by their cooling effects: lower temperatures generally lead to lower opacities in the UV, and a lower temperature allows more Ca III to recombine to Ca II. However, the cooling effects also introduced a new problem: the infrared triplet (IR3) of Ca II $\lambda\lambda$8498, 8542, 8662 (a trio of strong permitted lines) is responsible for the emission at 8600 Å, but the model overestimates the strength of the emission at this wavelength. In the observation, there is a pair of weaker emission features at the same location, and it is possible that at least one of these two emissions is due to the Ca II IR3, although probably not both, since they are spread too far apart in wavelength. It is therefore not entirely clear which of the two synthetic spectra is 'better',
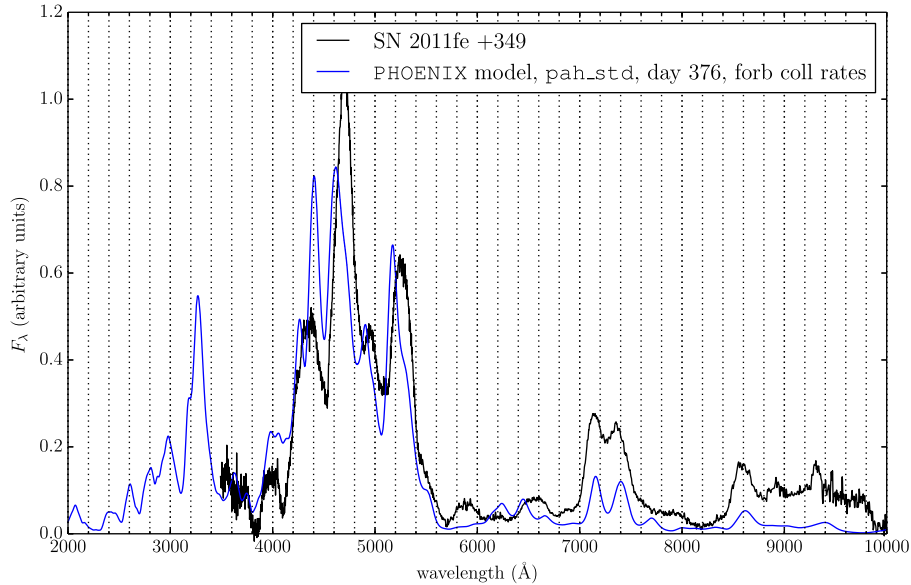
Figure 12. Synthetic spectrum of delayed-detonation model of Domínguez et al. (2001) at day +376 versus SN 2011fe at day +349. Permitted and forbidden lines were included in this calculation.

and it is possible, therefore, that both permitted and forbidden lines affect the optical spectra of SNe Ia at this epoch.

4.2 Day +205

The day +205 spectrum of SN 2011fe and the corresponding PHOENIX spectrum are shown in Fig. 8. Attempts to calculate a spectrum at this epoch without forbidden lines, as was done in Section 4.1, led to unrecoverable numerical instabilities in the code. It seems, then, that this age forbidden lines play an important role. The single-ion spectra are shown in Fig. 9. The emission feature at 4700 Å is primarily [Fe III] $\lambda\lambda 4607$, 4658 and [Fe II] $\lambda\lambda 4640$, 4664. The weak but clearly separate features around 4300 Å are [Fe II] $\lambda\lambda$ 4287, 4359, and the emission at 5300 Å is [Fe II] $\lambda 5300$. The double-horned feature in the synthetic spectrum centred around 7300 Å consists of [Fe II] $\lambda\lambda 7155$, 7172 on the left and [Ni II] $\lambda 7412$ on the right; the shape of this pair of features is too separated (unblended) in the synthetic spectrum compared to the day +100 spectrum of SN 2011fe, but at later epochs, the shape is a good match to the observations.

At this epoch, the ratio of Fe II to Fe III is reasonable, with the strength of the 4700 Å emission from Fe III improved over that from the day +100 spectrum. However, the 5200 Å emission, also from Fe III, is somewhat weak. The strong Ca II IR3 emission that was overestimated in strength in the day +100 synthetic spectrum is now absent entirely. Coincidentally, the forbidden line [Fe II] $\lambda 8617$, at nearly the same wavelength as IR3, has grown in strength at day +205, and fits quite well to the observation. The Ca II H&K doublet, which was quite strong at day +100, has diminished in strength and is replaced mostly by [Fe III] $\lambda 4008$. It seems, then, that the serendipitous degeneracy among permitted and forbidden lines, which Branch et al. (2005) found unlikely, may actually be realized, at least for some features in the optical spectra of SN 2011fe.

The double-horned pair of emissions centred at 7200 Å is better reproduced at this epoch as well. Now the emission at 5900 Å is quite well fitted with [Co III] $\lambda 5888$, while at day +100, when most

of the ^{56}Ni had decayed to ^{56}Co, the feature was absent entirely. It is possible that the temperature in the day +100 model was too low, which would explain the underabundance of Fe III emitting at 4700 Å and Co III emitting at 5900 Å. A higher temperature would also reduce the abundance of Ca II in favour of Ca III, explaining the reduced strength of both the H&K doublet and the IR3.

4.3 Day +311

The observed and synthetic spectra at day +311 are shown in Fig. 10, and the single-ion spectra are shown in Fig. 11. At this epoch, the spectra look similar to those at day +205. The [Fe III] emission at 4700 Å is still strong, although at day +311 the [Fe II] emission at 4400 Å has grown in strength, and continues to do so at later epochs. This is likely a reflection of some (but not much) recombination from Fe III to Fe II at this age. The Ca II H&K emission is still present at 4000 Å, but somewhat weak, just as at day +205.

4.4 Day +349

The model and observations at day +349 are displayed in Fig. 12. The corresponding single-ion spectra are shown in Fig. 13. The Ca II H&K doublet emission at 4000 Å is of similar strength as at day +205, and it may still contribute to that feature in SN 2011fe, although the [Fe III] appears to be stronger at that wavelength.

At this and later epochs, the model begins to exhibit some problems. A sharp emission feature forms in the near-UV in the synthetic spectrum that is not observed in SN 2011fe. In addition, in the synthetic spectrum the emission at 4400 Å (due mostly to Fe II) is nearly as strong as the 4700 Å feature (mostly Fe III), while in the observed spectrum the latter remains considerably stronger. This problem is likely not one of radiative transfer effects in the model, but rather one of atomic physics. The recombination rate for ions scales with the free-electron density n_e, which dilutes geometrically roughly as t^{-3} (De, Baron & Hauschildt 2010). Thus, at these very late times, the recombination time-scale for, say, Fe II can be of the same order as the dynamical time-scale (the age of the SN). In this case,
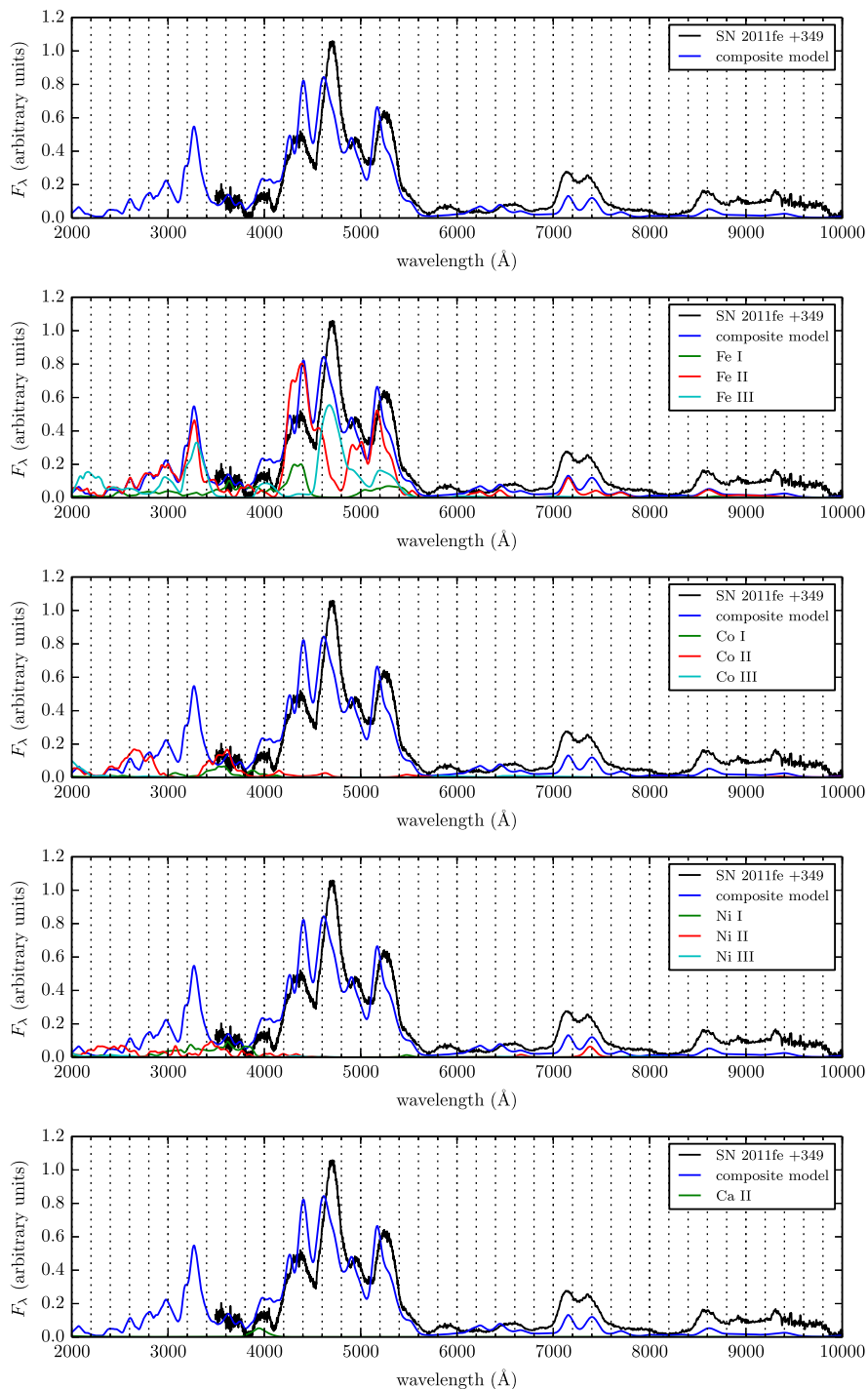
Figure 13. Single-ion spectra corresponding to the composite spectrum of the delayed-detonation model of Domínguez et al. (2001) at day +376 compared to SN 2011fe at day +349. Permitted and forbidden lines were included in this calculation.

time-dependent effects of ion recombination can become influential on spectrum formation (Sollerman et al. 2004; Taubenberger et al. 2015). In the calculations used to generate the above figures, we neglected time-dependence in both the radiation field and the ion populations: both are assumed to be in steady state.

While time-dependent effects in the ion populations are a possible source of discrepancy, there are other possibilities as well. The density profile of the ejecta in the explosion model also strongly affects n_e. Thus, the Fe II-to-Fe III population ratio may provide a constraint on the initial conditions of the explosion model. For example, Fig. 12 may indicate that the density of the iron-rich core of the model is too high, leading to an n_e that is too high, inducing recombination from Fe III to Fe II too soon.

Fransson & Jerkstrand (2015) found that time dependence was not very important for any of the epochs that we have studied; thus, it is more likely that the discrepancies we see with observations are due to inadequacies in the underlying explosion model.
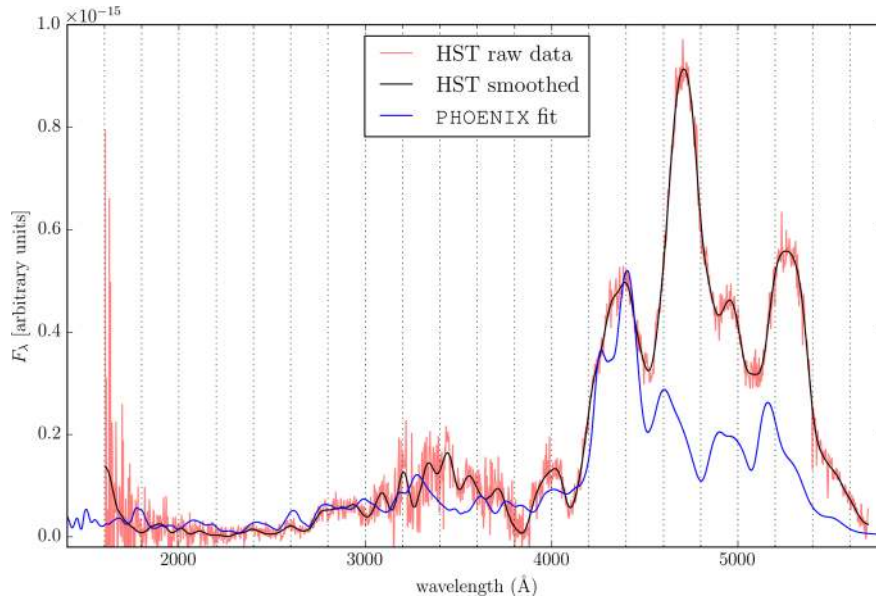
Figure 14. Synthetic spectrum of delayed-detonation model of Domínguez et al. (2001) at day +376 compared to SN 2011fe obtained with *HST* at day +360. Permitted and forbidden lines were included in this calculation.

4.5 The ultraviolet spectrum at day +360

The UV spectrum from *HST* at day +360, as well as the best-fitting spectrum from PHOENIX, are shown in Fig. 14. The single-ion spectra are shown in Fig. 15. From these, one finds that Fe II is responsible for most of the spectral features in the UV at day +360, just as it was at day +100. However, Fe III, Co III and Ni III all contribute significantly to the bluest portion of the spectrum as well. The most interesting result, however, is that the Ca II H&K doublet continues to contribute significantly to the emission around 4000 Å, despite being over 1 yr since explosion. It seems, then, that the extreme strength of this line overcomes both the small total abundance of Ca II in the ejecta, as well as the large amount of geometric dilution which accompanies a year of expansion.

A second notable feature of this result is that nearly all of the Fe II features are permitted lines, not forbidden; the bluest forbidden lines for any ion in this version of the PHOENIX atomic data base is about 3200 Å. Identifying these features is no simple feat, however, because Fe II has thousands of lines in the range of ∼1600–4000 Å. Furthermore, the contributions from other iron-group ions in the UV at late times, each with several thousands of lines themselves, are at some wavelengths of similar strength as Fe II. The convolution of all of these lines from different species renders the identification of individual features in the UV a difficult task. However, even without identifying particular lines, we can nevertheless learn a great deal about the UV line-forming region using other methods (see Fig. 6).

4.6 Day +578

Fig. 16 shows the observed and synthetic spectra of SN 2011fe at day +578. The single-ion spectra are displayed in Fig. 17. The fit of the PHOENIX synthetic spectrum to the observation is not adequate, and has resisted improvement even experimenting with a variety of different temperature-correction algorithms. Possible culprits for this include time-dependent effects as discussed in Section 4.4, as well as other physical processes that PHOENIX currently does not treat, including dielectric recombination and charge-exchange reactions. However, analysis of this result nevertheless reveals some useful information. For example, the unphysical spike in flux around 3250 Å is due entirely to Fe II, although to which line in particular is not clear. In addition, the emission at 8600 Å formerly produced by Ca II IR3 has been replaced by [Fe II] λ8617. This is yet another example of a truly remarkable degeneracy among permitted lines and forbidden lines at similar wavelengths, which become active at very different times.

Although our model spectra predict the recombination to Fe II too early, the event eventually does happen in SN 2011fe. In particular, in the day +594 spectrum, the strong Fe III emission peak at 4700 Å has disappeared entirely, with only a handful of Fe II features remaining. Indeed, Taubenberger et al. (2015) and Graham et al. (2015) have tentatively identified features of Fe I in the ∼1000 d spectrum of SN 2011fe, perhaps heralding a concurrent recombination transition from Fe II to Fe I.

5 VELOCITY SHIFTS

In a recent paper, Black, Fesen & Parent (2016) examined the wavelength shifts of several prominent blue features seen at late times in 27 SNe Ia, including SN 2011fe. They found a large and steady redward shift of the prominent 4700 Å feature and two other adjacent blue emission features in all SNe Ia in their sample with no sign of the redward drift slowing down at epochs up to day +400.

Fig. 18 indicates that our models show no such general trend for the 4700 Å feature. In fact, the 4700 Å feature after an initial strong redward shift begins to move back to the blue. Black et al. (2016) suggested that the ubiquitous redshift of these common late-time SN Ia spectral features is not mainly due to a decrease in line velocities of Fe III and Fe II line emissions as has been previously proposed (Maeda et al. 2011; Silverman et al. 2013), but likely the combined result of decreasing line velocities and opacity of permitted Fe absorption lines. Differences between our nebular models and the observed redshifts of late-time features in SN Ia spectra may simply reflect weaker contributions from forbidden-line emissions than assumed. Since these lines are very temperature sensitive, this could be indicative of our general model uncertainties.
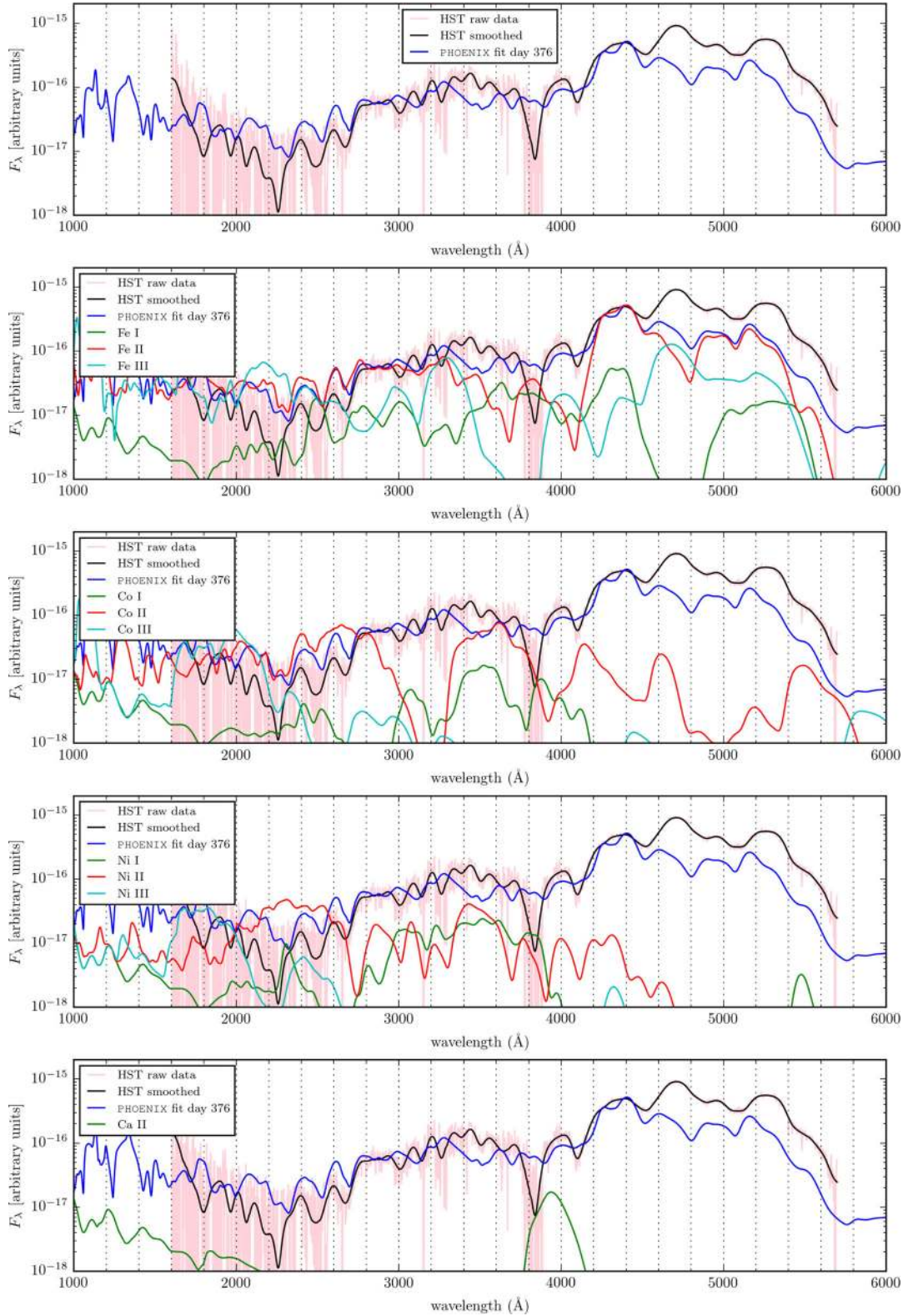
Figure 15. Single-ion spectra corresponding to the composite spectrum of the delayed-detonation model of Domínguez et al. (2001) at day +376 compared to SN 2011fe at day +360. Permitted and forbidden lines were included in this calculation.

6 OPACITY AT LATE TIMES

Our PHOENIX calculations have been fairly successful at reproducing the late-time optical and UV spectra of the normal SN 2011fe. In

addition, one of the great advantages of using first-principles codes such as PHOENIX is that one may glean a great deal of information about the underlying physics that drives the formation of the synthetic spectra. In Figs 19 and 20, we show the optical depths along
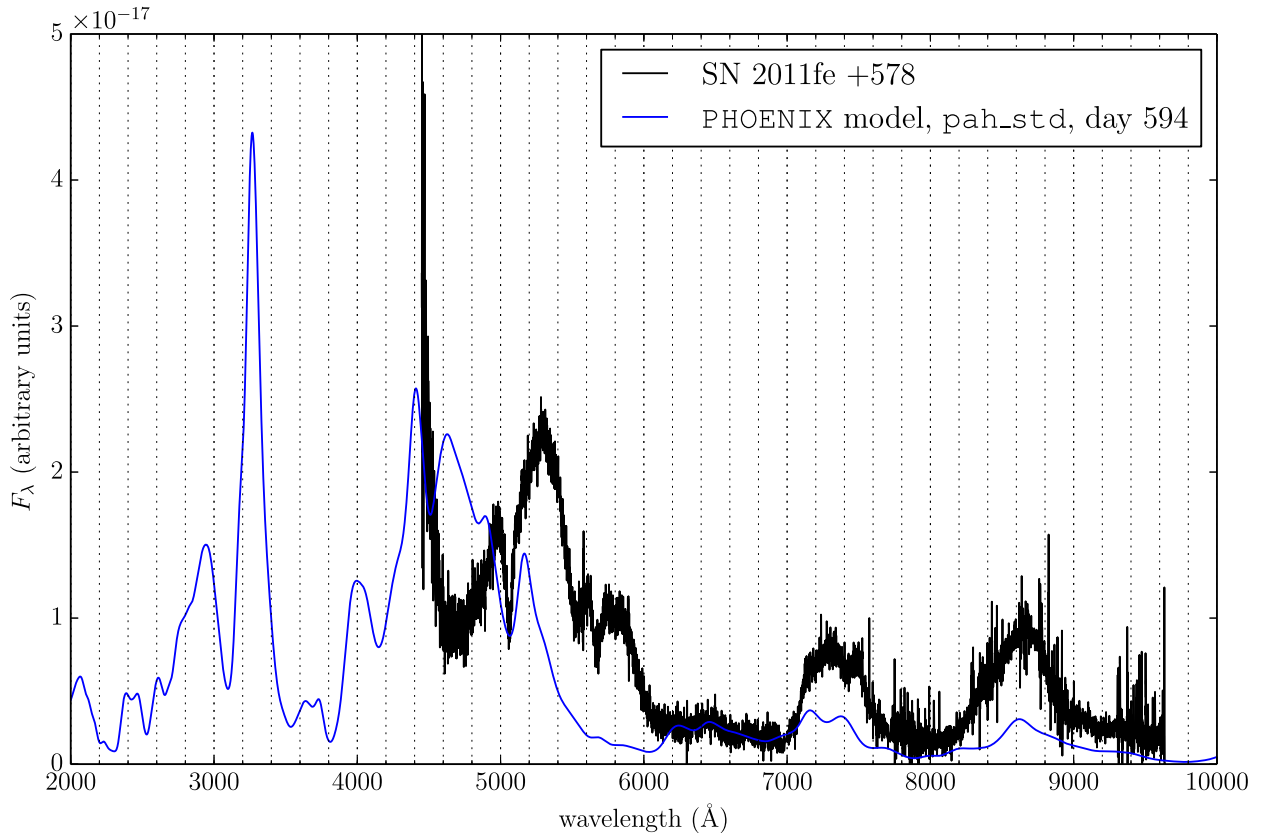
Figure 16. Synthetic spectrum of delayed-detonation model of Domínguez et al. (2001) at day +594 versus SN 2011fe at day +578. Permitted and forbidden lines were included in this calculation.

the $\mu = -1$ (radially inward) ray in the day +100 and day +349 models. For reference, the black dashed line shows $\tau = 1$, the division between optically thick and optically thin. The dashed red line displays the optical depth due only to Thomson scattering; at early times, this is the dominant opacity source and gives rise to the photosphere in SNe. At late times, however, the geometric dilution of the free-electron density n_e leads to a very low Thomson scattering opacity, falling well below $\tau = 1$ even all the way to the centre of the ejecta. From this alone we may infer that there is likely very little continuum radiation present this late in a SN Ia's lifetime, as reflected in the spectra. Furthermore, at only a select few wavelengths – mostly on the blue edge of the optical band – does the optical depth reach $\tau = 1$ at all; at most wavelengths $\lambda \gtrsim 4500\,\text{Å}$, the ejecta are quite optically thin, in agreement with previous studies. Our calculations, therefore, indicate that most of the optical spectra at day +349 in SN 2011fe consist of blended emission features from collisionally excited, optically thin forbidden lines.

The UV portion of the spectrum of SN 2011fe, however, behaves entirely differently than the optical. Figs 21 and 22 show the optical depths along $\mu = -1$ in the UV for days +100 and +349. One may suspect as much simply by noticing the significant degree of structure and complexity in the observed UV spectrum (Fig. 2). These suspicions are confirmed by analogous calculations of optical depths at various UV wavelengths, shown in Fig. 22. The black and red dashed lines are the same as in Fig. 20. Unlike the optical band, however, most UV wavelengths are *extremely* optically thick, with many reaching $\tau \sim 10^5$ at the centre of the ejecta. Another surprising result is that many UV wavelengths become optically

thick at quite high velocity, crossing the $\tau = 1$ threshold at $v \approx$ 10 000–15 000 km s^{-1}. This result is corroborated by the presence of the emission component of the Ca II H&K doublet near 4000 Å in Fig. 15.

If the UV remains as optically thick as Figs 20 and 22 suggest, then it appears that the transition from the 'photospheric' to the 'nebular' phase in SNe Ia is far more complex than expected. Specifically, there are likely few or no forbidden emission lines that are active in the UV; this precludes the possibility of measuring asymmetric bulk motion of the inner regions of the SN ejecta, since the assumption behind such measurements is that the emission lines are optically thin and centred at the line rest wavelengths (Maeda et al. 2010). On the other hand, since the UV is optically thick, the spectrum may consist of the same overlapping P Cygni line-scattering profiles that characterize maximum-light spectra of SNe; if this is the case, we may be able to infer ejecta velocities of the iron-rich core of SN 2011fe by measuring the location of the absorption minima of the features in Fig. 2. However, as discussed in Section 4.5, the multitude of UV lines, as well as likely blending among several atomic species, make this challenging. If we entertain the possibility that some of the UV spectrum is forming at the UV photosphere at velocities of order 10 000 km s^{-1}, the rest wavelengths of such lines would still lie within a crowded space of UV and optical transitions of iron-peak elements.

Of course, as the supernova expands, forbidden lines become more important, as is clear already by day +205, where forbidden lines were absolutely required. The important point is that permitted lines are important as well.
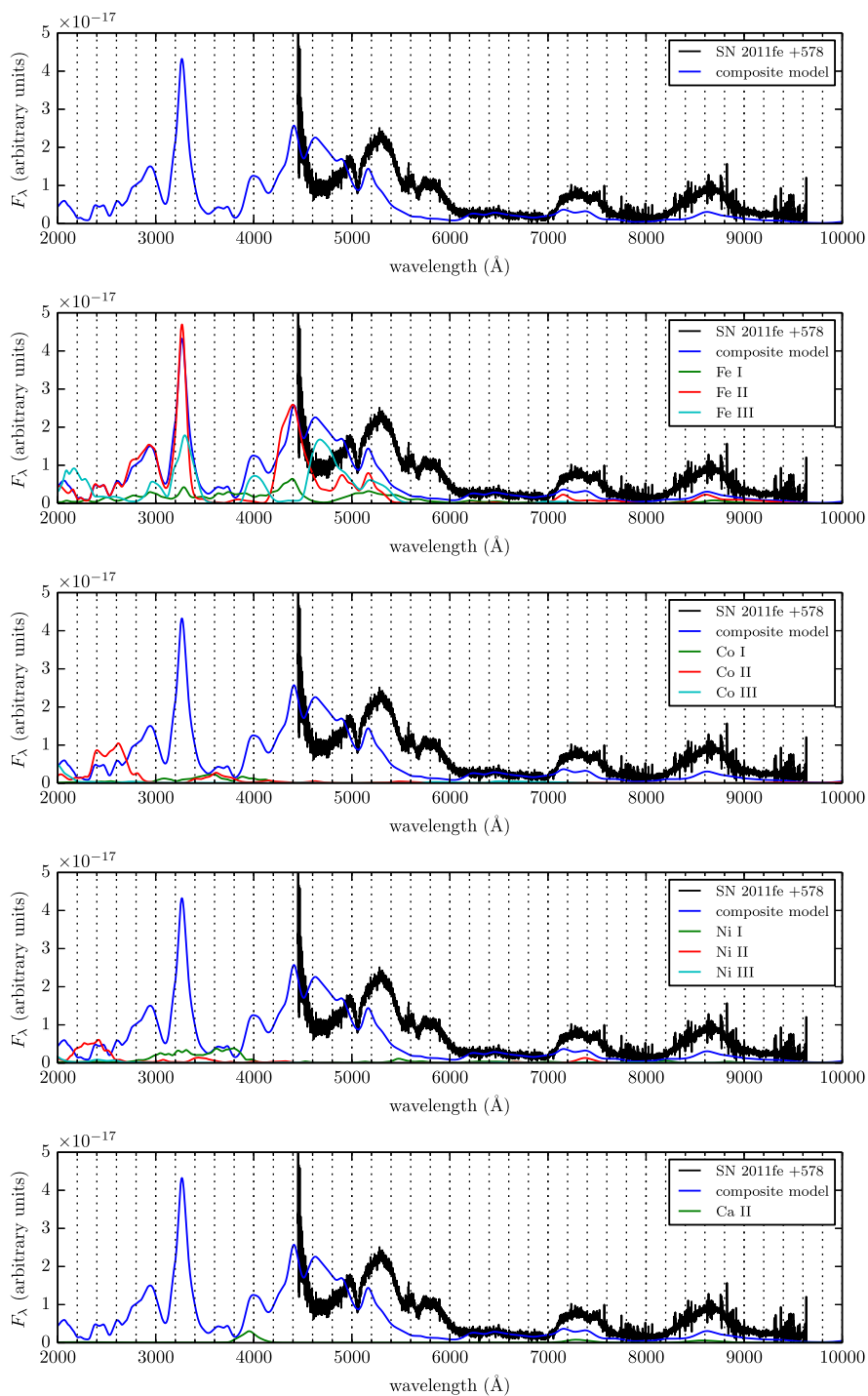
Figure 17. Single-ion spectra corresponding to the composite spectrum of the delayed-detonation model of Domínguez et al. (2001) at day +594 compared to SN 2011fe at day +578. Permitted and forbidden lines were included in this calculation.

7 CONCLUSIONS

We extended PHOENIX to calculate radiative transfer models well into the late-time epochs of SNe Ia, with an eye towards obtaining fits to the high-quality optical and UV spectra of SN 2011fe. Doing so required similar methods to those discussed by Friesen et al. (2014), in particular, using an alternative method to that of Unsöld-Lucy (Lucy 1964) for calculating the temperature structure of the gas, as well as accounting for the collisional and radiative rate data

for forbidden lines, which behave quite differently than permitted lines. The resulting synthetic spectra, ranging from +100 to +578 d post-maximum light, vary in degrees of fidelity to corresponding observed spectra of SN 2011fe, with the earlier epochs fitting quite well and the later epochs less so. At day +100, we found that radiative transfer calculations that neglect forbidden lines and those that include them can produce remarkably similar optical spectra, but with quite different atomic species and combinations of lines forming the various features. We found that, at least as late as
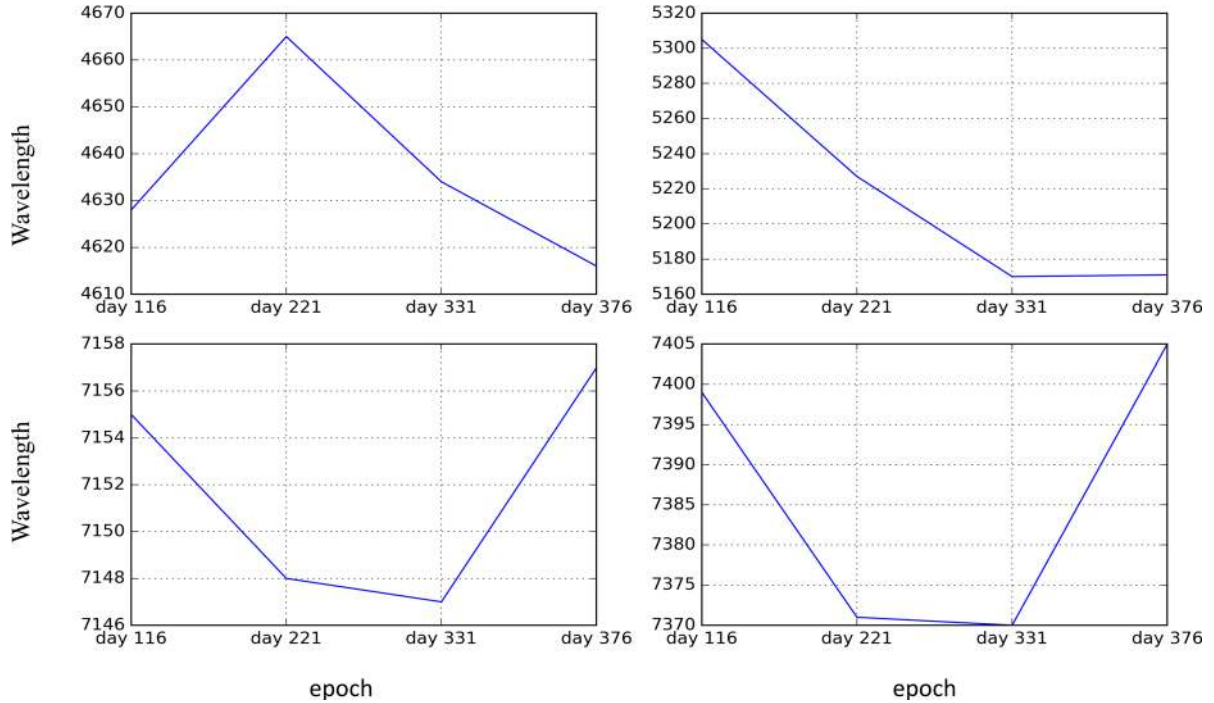
Figure 18. The position of the central wavelength peak of the 4700, 5300, 7150 and 7400 Å features (clockwise from upper left) as a function of epoch.
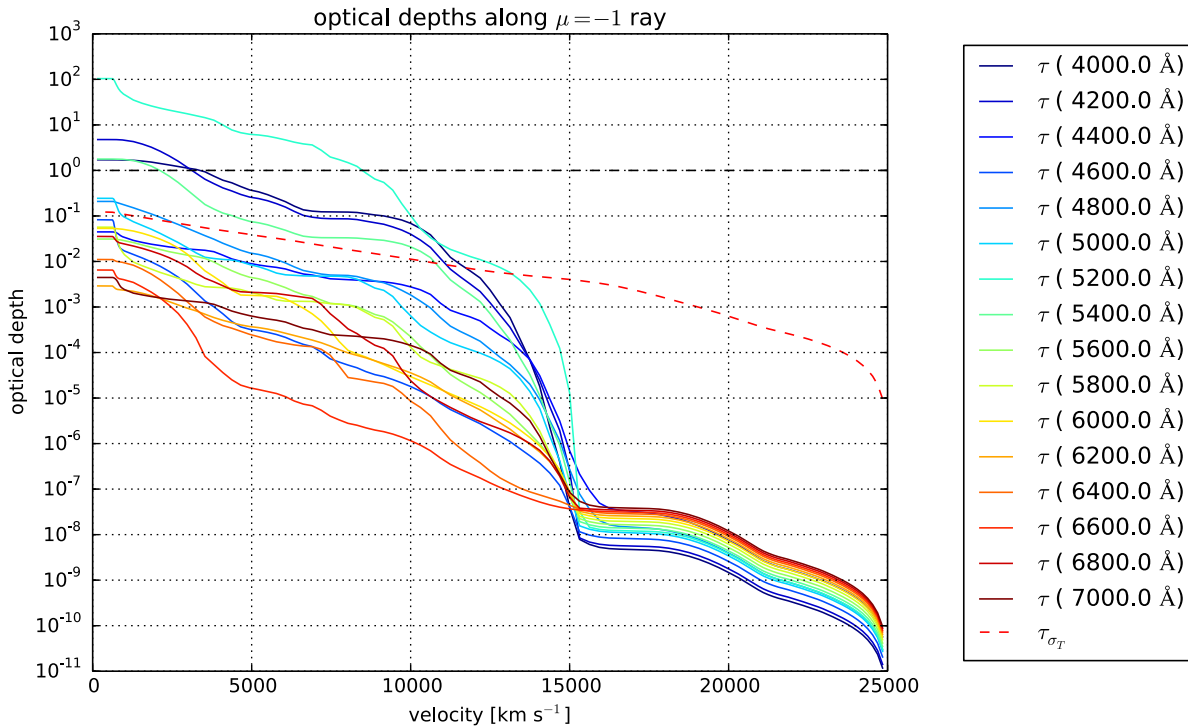
Figure 19. Optical depths at a collection of optical wavelengths in the day +100 model (cf. Fig. 5).

day +360, permitted lines such as Ca II H&K and IR3 continue to influence spectrum formation in the optical, and permitted lines of Fe II form much of the spectrum in the UV. In addition, these models indicate that some emission features from permitted lines are replaced by other emission features of forbidden lines at nearly the same wavelength as the SN evolves. For example, the emission from Ca II H&K at 4000 Å is replaced around day +205 by [Fe III] λ4008, and the emission from Ca II IR3 at around 8600 Å is replaced by [Fe II] λ8617.

Our results on the importance of permitted lines are in general agreement with those of other late-time studies of other groups (Jerkstrand, Fransson & Kozma 2011; Fransson & Jerkstrand 2015),
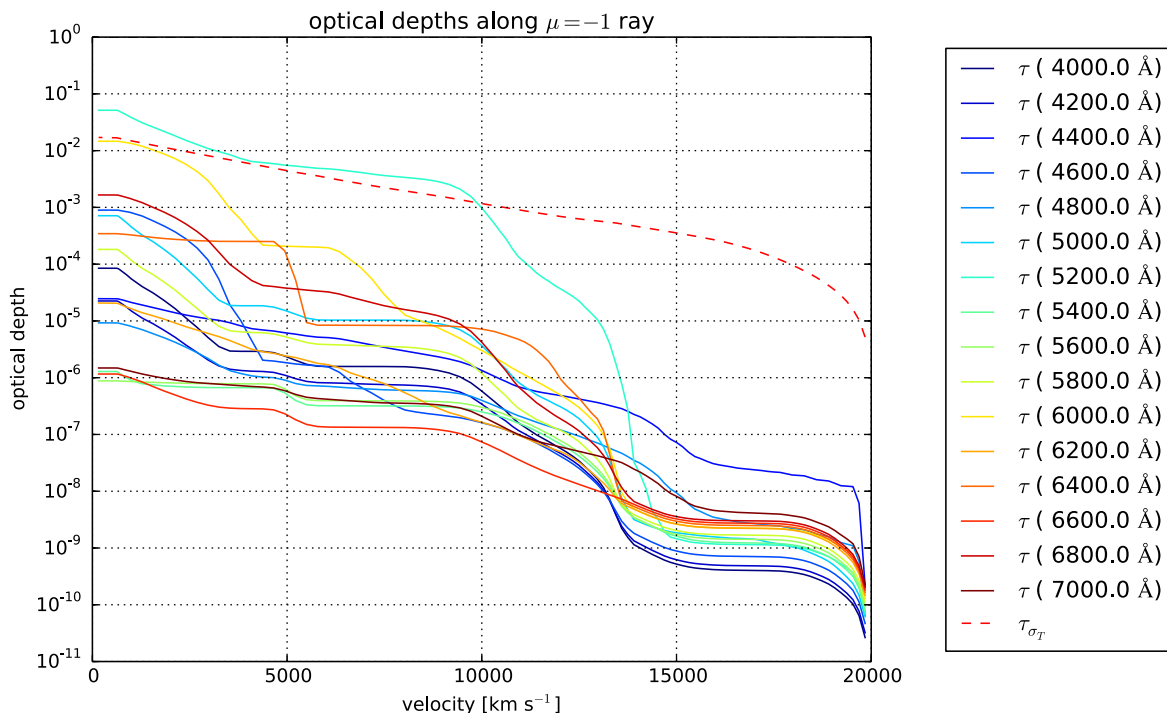
Figure 20. Optical depths at a collection of optical wavelengths in the day +349 model (cf. Fig. 12)
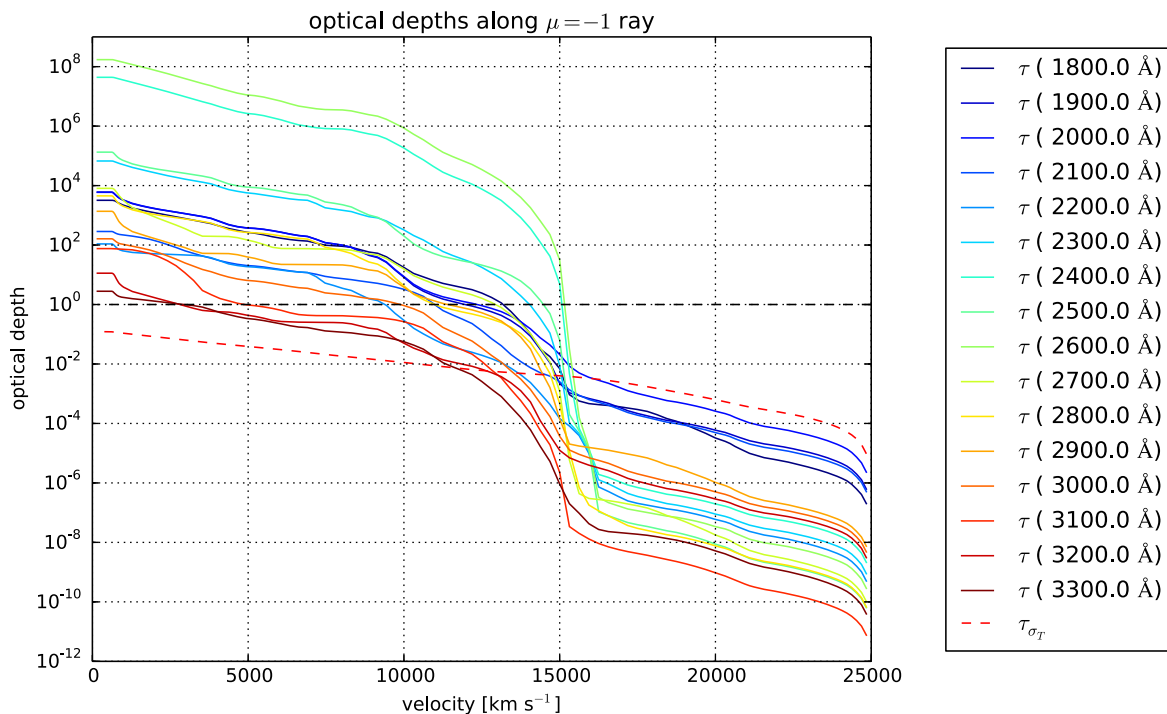
Figure 21. Optical depths at a collection of UV wavelengths in the day +100 model (cf. Fig. 5).

and we find in agreement with Mazzali et al. (2015) that a nickel hole is required – that is, there was neutronization in the very centre of the ejecta.

Figure 22. Optical depths at a collection of UV wavelengths in the day +349 model (cf. Fig. 12).

REFERENCES

Axelrod T. S., 1980, PhD thesis, Univ. California, Santa Cruz
Black C. S., Fesen R. A., Parrent J. T., 2016, MNRAS, 462, 649
Bloom J. S. et al., 2012, ApJ, 744, L17
Bongard S., Baron E., Smadja G., Branch D., Hauschildt P. H., 2008, ApJ, 687, 456
Bowers E. J. C., Meikle W. P. S., Geballe T. R., Walton N. A., Pinto P. A., Dhillon V. S., Howell S. B., Harrop-Allin M. K., 1997, MNRAS, 290, 663
Branch D., Baron E., Hall N., Melakayil M., Parrent J. T., 2005, PASP, 117, 545
Branch D. et al., 2008, PASP, 120, 135
Childress M. J. et al., 2015, MNRAS, 454, 3816
Chomiuk L. et al., 2012, ApJ, 750, 164

De S., Baron E., Hauschildt P. H., 2010, MNRAS, 401, 2081
Dessart L., Hillier D. J., Blondin S., Khokhlov A., 2014, MNRAS, 439, 3114
Domínguez I., Höflich P., Straniero O., 2001, ApJ, 557, 279
Fransson C., Jerkstrand A., 2015, ApJ, 814, L2
Friesen B., Baron E., Branch D., Chen B., Parrent J. T., Thomas R. C., 2012, ApJS, 203, 12
Friesen B., Baron E., Wisniewski J. P., Parrent J. T., Thomas R. C., Miller T. R., Marion G. H., 2014, ApJ, 792, 120
Graham M. L., Nugent P. E., Sullivan M., Filippenko A. V., Cenko S. B., Silverman J. M., Clubb K. I., Zheng W., 2015, MNRAS, 454, 1948
Graur O., Maoz D., Shara M. M., 2014, MNRAS, 442, L28
Hauschildt P. H., Baron E., 1999, J. Comput. Appl. Math., 109, 41
Hauschildt P. H., Baron E., 2014, A&A, 566, A89
Horesh A. et al., 2012, ApJ, 746, 21
Iwamoto K., Brachwitz F., Nomoto K., Kishimoto N., Umeda H., Hix W. R., Thielemann F.-K., 1999, ApJS, 125, 439
Jerkstrand A., Fransson C., Kozma C., 2011, A&A, 530, A45
Jha S., Branch D., Chornock R., Foley R. J., Li W., Swift B. J., Casebeer D., Filippenko A. V., 2006, AJ, 132, 189
Kerzendorf W. E., Taubenberger S., Seitenzahl I. R., Ruiter A. J., 2014, ApJ, 796, L26
Kirshner R. P., Oke J. B., 1975, ApJ, 200, 574
Kuchner M. J., Kirshner R. P., Pinto P. A., Leibundgut B., 1994, ApJ, 426, L89
Kurucz R. L., 1995, in Adelman S. J., Wiese W. L., eds, ASP Conf. Ser. Vol. 78, Astrophysical Applications of Powerful New Databases. Astron. Soc. Pac., San Francisco, p. 205
Kurucz R. L., 2002, in Schultz D. R., Krstic P. S., Ownby F., eds, AIP Conf. Ser. Vol. 636, Atomic and Molecular Data and Their Applications. Am. Inst. Phys., New York, p. 134
Li W. et al., 2011, Nature, 480, 348
Lucy L. B., 1964, SAO Spec. Rep., 167, 93
Lundqvist P. et al., 2015, A&A, 577, A39
Maeda K. et al., 2010, Nature, 466, 82
Maeda K. et al., 2011, MNRAS, 413, 3075
Margutti R. et al., 2012, ApJ, 751, 134

Marion G. H., Höflich P., Gerardy C. L., Vacca W. D., Wheeler J. C., Robinson E. L., 2009, AJ, 138, 727

Mazzali P. A., Hachinger S., 2012, MNRAS, 424, 2926

Mazzali P. A., Sauer D. N., Pastorello A., Benetti S., Hillebrandt W., 2008, MNRAS, 386, 1897

Mazzali P. A., Maurer I., Stritzinger M., Taubenberger S., Benetti S., Hachinger S., 2011, MNRAS, 416, 881

Mazzali P. A. et al., 2014, 439, 1959

Mazzali P. A. et al., 2015, MNRAS, 450, 2631

McClelland C. M., Garnavich P. M., Milne P. A., Shappee B. J., Pogge R. W., 2013, ApJ, 767, 119

Meyerott R. E., 1978, ApJ, 221, 975

Meyerott R. E., 1980, ApJ, 239, 257

Munari U., Henden A., Belligoli R., Castellani F., Cherini G., Righetti G. L., Vagnozzi A., 2013, New A, 20, 30

Nomoto K., Thielemann F.-K., Yokoi K., 1984, ApJ, 286, 644

Nugent P. E. et al., 2011, Nature, 480, 344

Parrent J. T. et al., 2012, ApJ, 752, L26

Pereira R. et al., 2013, A&A, 554, A27

Piro A. L., Nakar E., 2014, ApJ, 784, 85

Richmond M. W., Smith H. A., 2012, J. Am. Assoc. Var. Star Obs. (JAAVSO), 40, 872

Röpke F. K. et al., 2012, ApJ, 750, L19

Ruiz-Lapuente P., Kirshner R. P., Phillips M. M., Challis P. M., Schmidt B. P., Filippenko A. V., Wheeler J. C., 1995, ApJ, 439, 60

Ruiz-Lapuente P., Lucy L. B., 1992, ApJ, 400, 127

Shappee B. J., Stanek K. Z., Pogge R. W., Garnavich P. M., 2013, ApJ, 762, L5

Silverman J. M., Ganeshalingam M., Filippenko A. V., 2013, MNRAS, 430, 1030

Sollerman J. et al., 2004, A&A, 428, 555

Taubenberger S. et al., 2015, MNRAS, 448, L48

Thomas R. C., Nugent P. E., Meza J. C., 2011, PASP, 123, 237

Vinkó J. et al., 2012, A&A, 546, A12

This paper has been typeset from a TEX/LATEX file prepared by the author.